Three-Dimensional Reconstruction of Objects Embedded in Spherically Layered Media Using Variational Born Iterative Method

Yongjin Chen, Paiju Wen, Feng Han, Na Liu, Hai Liu, *Member, IEEE*, and Qing Huo Liu, *Fellow, IEEE*

***Abstract*— The variational Born iterative method (VBIM) is employed here to reconstruct 3-D objects with permittivity contrast buried in spherically multilayered media. The nonlinear inverse problem is solved iteratively via the conjugate-gradient method, and in each iteration, the scattered field is linearized by using the Born approaximation. The forward solver is provided by the method of moments combined with a Krylov subspace method. The dyadic Green's function for spherically layered media is constructed in terms of the spherical vector wave functions by using the scattering superposition in the spherical coordinate system and then transformed into the Cartesian coordinate system. Thus, the inversion region is discretized into *N* uniform cubic cells and the reconstructed result can be obtained in the Cartesian coordinate system by employing VBIM. Numerical results with high resolution are presented to validate the capability of our method in reconstructing 3-D multiple objects of arbitrary shapes buried in spherically multilayered media.**

***Index Terms*— Biconjugate-gradient stabilized algorithm (BCGS), inverse scattering, permittivity contrast, spherically layered media, variational Born iterative method (VBIM).**

I. Introduction

THREE-dimensional reconstruction of inhomogeneous objects of arbitrary shapes using electromagnetic (EM) waves has a history of several decades. However, it is still a challenge to solve the EM inverse scattering problem in a stable and high-efficient way due to its nonlinearity and ill-posedness. To overcome those difficulties, several research groups proposed various linear [1]–[5] and nonlinear methods [6]–[11]. Wang and Chew [12] reconstructed the permittivity by employing the Born iterative method (BIM). They also suggested the distorted BIM (DBIM) for inverse scattering problems [13], which was further validated by several numerical experiments based on laboratory measured data [14]. Zaiping and Yerong [15] developed a hybrid BIM (HBIM), in which DBIM was used in the first several iterative steps to gain the fast convergence while in the last several steps BIM was applied to make the solution more stable. However, the dyadic Green's functions must been calculated for each iteration in DBIM which is time consuming. Moreover, switching from DBIM to BIM is not very convenient due to the difference of two methods. Thus, Zaiping *et al.* [16] suggested the variational BIM (VBIM) to reduce the computation cost of DBIM and improve the switching to BIM in 2-D media. Zhang and Liu [17] have successfully applied the VBIM in simultaneous reconstruction of permittivity and permeability contrasts. Up to now, there are several research groups working on the 3-D reconstruction in a homogeneous [14], [16] or a planarly layered medium [18], [19] background. However, 3-D inverse scattering from objects with electric contrast in spherically layered media has not been studied, although it has many potential applications such as geophysical exploration, ionosphere detection, planet exploration, and atmosphere characterization.

In this letter, we will focus on the 3-D reconstruction of objects buried in spherically layered media by employing the VBIM due to its stability and high-efficiency compared with HBIM. The nonlinear inverse problem is solved iteratively by conjugate-gradient (CG) method [20], and in each iteration, it is linearized by Born approximation. In each inversion iteration, a numerical forward solver based on the method of moments (MOM) [21], [22] combined with the Krylov subspace method is provided. In the forward solver, the dyadic Green's function in spherically layered media is first computed in the spherical coordinate system and later transformed into the Cartesian coordinate system.

This letter is organized as follows. In Section I, we give a brief introduction of the forward and inverse problem formulations. The reconstructed results with one or two objects buried in a three spherically layered medium are presented in Section III, followed by conclusions in Section IV.

II. Theory

Fig. 1 shows a typical model of 3-D scattering and inverse scattering in spherically layered media, where one or multiple inhomogeneous dielectric objects of arbitrary shapes are completely buried in a spherically layered medium that has m layers with independent permittivity, conductivity, and permeability $(\epsilon_i, \sigma_i, \mu_i)$. The complex permittivity is expressed as $\tilde{\epsilon} = \epsilon + \sigma/j\omega$. The inversion region containing all the scatters is denoted by D in the bth layer. The background permittivity, conductivity, and permeability of the bth layer are ϵ_b, μ_b, σ_b, respectively. The electrical properties of the scatter are $\epsilon(\mathbf{r})$,

Manuscript received November 15, 2016; revised January 18, 2017 and March 8, 2017; accepted April 9, 2017. Date of publication May 3, 2017; date of current version June 22, 2017. This work was supported in part by the National Natural Science Foundation of China under Grant 41390453 and 41504120. *(Corresponding author: Feng Han.)*

Y. Chen, P. Wen, F. Han, N. Liu, and H. Liu are with the Department of Electronic Science, Institute of Electromagnetics and Acoustics, Xiamen University, Fujian 361005, China (e-mail: feng.han@xmu.edu.cn).

Q. H. Liu is with the Department of Electrical and Computer Engineering, Duke University, Durham, NC 27708 USA (e-mail: qhliu@duke.edu).

Color versions of one or more of the figures in this letter are available online at http://ieeexplore.ieee.org.

Digital Object Identifier 10.1109/LGRS.2017.2694007

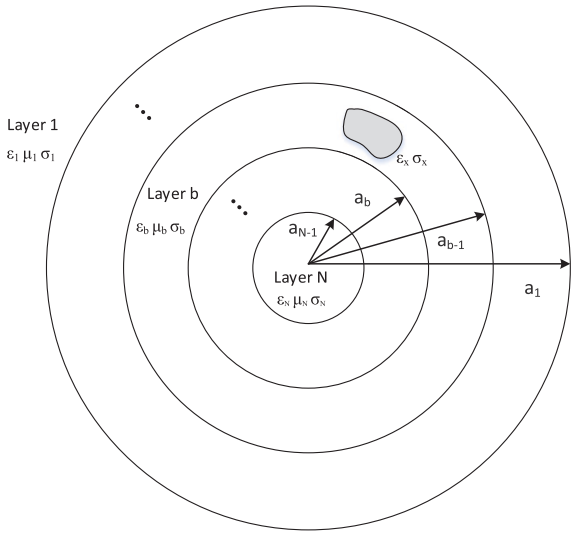

Fig. 1. Typical configuration of an inhomogeneous object buried in spherically multilayered media.

$\sigma(\mathbf{r})$, and μ_b, i.e., we only consider the electric contrast which is more common in reality.

A. Forward Problem Formulation

As illustrated in Fig. 1, in a spherically layered medium, an inhomogeneous dielectric object with an arbitrary shape is completely buried in the bth layer. The scattered field $\mathbf{E}^{\text{scat}}(\mathbf{r})$ is the difference between the total electric field $\mathbf{E}(\mathbf{r})$ and the incident field $\mathbf{E}^{\text{inc}}(\mathbf{r})$, or

$$\mathbf{E}^{\text{scat}}(\mathbf{r}) = \mathbf{E}^{\text{tot}}(\mathbf{r}) - \mathbf{E}^{\text{inc}}(\mathbf{r}) \tag{1}$$

where $\mathbf{r}$ is the position vector in the 3-D space and $\mathbf{E}^{\text{inc}}(\mathbf{r})$ is the electric field in the absence of the scatterer but with the existence of the spherically layered background medium.

According to the volume equivalence theorem, the scattered field satisfies the following equation:

$$\mathbf{E}^{\text{scat}}(\mathbf{r}) = \int_D \overline{\mathbf{G}}_{\text{EJ}}(\mathbf{r}, \mathbf{r}') \cdot \mathbf{J}_{\text{eq}}(\mathbf{r}') d\mathbf{r}' \tag{2}$$

where $\overline{\mathbf{G}}_{\text{EJ}}(\mathbf{r}, \mathbf{r}')$ is the electric dyadic Green's function in the spherically layered medium and denotes the electric field at $\mathbf{r}$ caused by a point electric dipole at the position of $\mathbf{r}'$. The general expression of $\overline{\mathbf{G}}_{\text{EJ}}$ in spherically layered media can be found in [23].

The volume equivalent current $\mathbf{J}_{\text{eq}}(\mathbf{r}')$ inside the inversion region is proportional to the total electric field, and is expressed as

$$\mathbf{J}_{\text{eq}}(\mathbf{r}') = j\omega\epsilon_b \chi_\epsilon(\mathbf{r}') \mathbf{E}^{\text{tot}}(\mathbf{r}') \tag{3}$$

where $\chi_\epsilon(\mathbf{r}') = [\epsilon(\mathbf{r}') - \epsilon_b(\mathbf{r}')]/\epsilon_b(\mathbf{r}')$ stands for the electric contrast, and the subscript b represents the bth layer of a multilayered medium.

By combining (1) and (2), we can obtain the following equation:

$$\mathbf{E}^{\text{inc}}(\mathbf{r}) = \mathbf{E}^{\text{tot}}(\mathbf{r}) - \omega^2 \mu_b \epsilon_b \int_D \overline{\mathbf{G}}_{\text{EJ}}(\mathbf{r}, \mathbf{r}') \cdot \chi_\epsilon(\mathbf{r}') \mathbf{E}^{\text{tot}}(\mathbf{r}') d\mathbf{r}. \tag{4}$$

In order to solve the volume integral equation above, we need to transform it into a discrete linear system. For convenience, we assume that the inversion region D containing the objects is divided into $N = N_x \times N_y \times N_z$ uniform cells. The pulse function is used as the basis function, i.e., the electric field at the center of each cell represents the mean value of the whole cell. In addition, the Green's function $\overline{\mathbf{G}}_{\text{EJ}}$ given in [23] is in the spherical coordinate system, so we transform it into the Cartesian coordinate system by applying the coordinate transform matrix.

In this way, the discretized volume integral equation can be solved by MOM combined with a Krylov subspace iteration method. In this letter, we chose the bicongugate-gradient stabilized (BCGS) algorithm due to its stabilization and rapid convergence.

B. Inverse Problem Formulation

Once the total electric field in the inversion region is solved by MOM combined with Krylov subspace iterative method, the scattered electric field at the receivers can be obtained from the following equation:

$$\mathbf{E}^{\text{scat}}(\mathbf{r}, \mathbf{r}_T) = j\omega\epsilon_b \int_D \overline{\mathbf{G}}_{\text{EJ}}(\mathbf{r}, \mathbf{r}') \cdot \chi_\epsilon(\mathbf{r}') \mathbf{E}^{\text{tot}}(\mathbf{r}', \mathbf{r}_T) d\mathbf{r}' \tag{5}$$

where $\mathbf{r}$ and $\mathbf{r}_T$ denote the vector position of receivers and transmitters, respectively. $\mathbf{E}^{\text{scat}}(\mathbf{r}, \mathbf{r}_T)$ represents the scattered field at the position of $\mathbf{r}$ caused by the transmitter at $\mathbf{r}_T$.

We performed several numerical experiments, and the results show that VBIM has less computation burden compared with DBIM and converges faster than BIM. Therefore, we choose VBIM as the inversion algorithm in this letter. We first take a variation on (5) and obtain the following equation:

$$\delta\mathbf{E}^{\text{scat}}(\mathbf{r}, \mathbf{r}_T) = j\omega\epsilon_b \int_D \overline{\mathbf{G}}_{\text{EJ}}(\mathbf{r}, \mathbf{r}') \cdot \delta\chi_\epsilon(\mathbf{r}') \mathbf{E}^{\text{tot}}(\mathbf{r}', \mathbf{r}_T) d\mathbf{r}' \tag{6}$$

where

$$\delta\mathbf{E}^{\text{scat}}(\mathbf{r}, \mathbf{r}_T) = \mathbf{E}^{\text{scat}}_{\text{meas}}(\mathbf{r}, \mathbf{r}_T) - \mathbf{E}^{\text{scat(k-1)}}(\mathbf{r}, \mathbf{r}_T) \tag{7}$$

denotes the difference between the measured scattered electric field and the calculated electric field at the $(k-1)$th iteration, and

$$\delta\chi_\epsilon(\mathbf{r}') = \chi_\epsilon^k(\mathbf{r}') - \chi_\epsilon^{(k-1)}(\mathbf{r}') \tag{8}$$

stands for the difference of electric contrast between the kth and $(k-1)$th iterations.

To solve $\delta\chi_\epsilon$ in (6), we need to transform it into a discrete system. The discretized equation can be expressed as

$$\delta\mathbf{f} = \mathbf{A}\delta\mathbf{x} \tag{9}$$

where $\delta\mathbf{f}$ and $\delta\mathbf{x}$ are column vectors representing discretized $\delta\mathbf{E}^{\text{scat}}$ and $\delta\chi_\epsilon$, respectively. $\mathbf{A}$ is a matrix in which each element is a function of volume of cell, total electric field, and the dyadic Green's function. The full expression of $\mathbf{A}$ can be found in [17]. The ill-posed (9) can be solved by applying

the Tikhonov regularization method. The cost function for the VBIM is defined as

$$\mathbf{F}_{n+1} = \frac{||\delta \mathbf{f}_n - \mathbf{A}\delta\chi_{n+1}||^2}{||\mathbf{f}_n||^2} + \gamma^2 \frac{||\delta\chi_{n+1}||^2}{||\chi_n||^2} \tag{10}$$

where $||\ \ ||$ denotes the L_2 norm. The minimization of the cost function is equivalent to solving the following equation [17]:

$$(\mathbf{A}^\dagger\mathbf{A} + \frac{\gamma^2||\mathbf{f}_n||^2}{||\chi_n||^2}\mathbf{I})\delta\chi_{n+1} = \mathbf{A}^\dagger\delta\mathbf{f}_n \tag{11}$$

where $\dagger$ represents the complex conjugate and the transpose. The CG method [20] is chosen here to solve this equation. After we obtain $\delta\chi_\epsilon$ at the nth step, both $\mathbf{E}^{\text{tot}}_{n+1}$ and $\mathbf{E}^{\text{scat}}_{n+1}$ can be calculated by the forward solver. Thus, if the updated $\delta\mathbf{E}^{\text{scat}}$ is not smaller than the prescribed threshold, we update the matrix $\mathbf{A}$ using $\mathbf{E}^{\text{tot}}_{n+1}$ and solve (11) again. In this way, the contrast χ_ϵ can be iteratively updated until the residual relative error of $\mathbf{E}^{\text{scat}}$ converges. At last, we can reconstruct permittivity and conductivity from the final value of χ_ϵ.

III. Numerical Results

In this section, we present some numerical results to validate the effectiveness of our method in reconstructing objects with electric contrast in spherically layered media.

We consider a three spherically layered medium and the space is characterized by $\epsilon_{r1} = 1.0$, $\mu_{r1} = 1.0$, $\sigma_1 = 0.0$ S/m, $r_1 = 10.0$ m; $\epsilon_{r2} = 2.0$, $\mu_{r1} = 1.0$, $\sigma_1 = 0.001$ S/m, $r_2 = 5.0$ m; and $\epsilon_{r3} = 4.0$, $\mu_{r3} = 1.0$, $\sigma_3 = 0.001$ S/m. The operating frequency used here is 30 MHz. The measured data used in the inversion are computed by our forward solver BCGS, which have been validated by full wave simulations [24]. In this letter, we only demonstrate the reconstruction results for the case in which the inversion region is located in the middle layer of a three spherically layered medium, though we can reconstruct the permittivity and conductivity in any layer. The typical configuration of transmitters and receivers is shown in Fig. 2. Six transmitters illuminate the inversion region in six directions. Receivers randomly distribute in a sphere shell covering the inversion region. Both receivers and sources are distributed in the middle layer.

To evaluate the accuracy of the reconstructed results, we define the relative error metric (REM) as

$$\text{REM} = \frac{||\boldsymbol{\epsilon}_{\text{retrieved}} - \boldsymbol{\epsilon}_{\text{true}}||}{||\boldsymbol{\epsilon}_{\text{true}}||} \tag{12}$$

where $\boldsymbol{\epsilon}_{\text{retrieved}}$ stands for the retrieved complex permittivity and $\boldsymbol{\epsilon}_{\text{true}}$ denotes the true complex permittivity in the inversion region. In the following, we retrieve the permittivity values in the inversion region by using both VBIM and BIM and compare their REMs.

A. Cube Buried in the Middle Layer of a Three-Layered Medium

In the first example, a homogeneous cubic scatterer with $\epsilon_{rx} = 4.0$, $\mu_{rx} = 1.0, and \sigma_x = 0.002$ S/m is buried in the middle layer. The center of the scatterer is located at $(4.55, 4.55, 4.55)$ m. The dimension of the scatterer is $L_x = L_y = L_z = 0.5$m. The inversion region D containing the scatterer is also a cubic region with one lower corner located in $(4.0, 4.0, 4.0)$ m and the opposite upper corner located in $(5.1, 5.1, 5.1)$ m. Thus, the object is at the center of the inversion region in the middle layer. In order to get enough information about the inversion region, we place 6 electric dipole sources at the same distance from the centers of six surfaces of D domain and 20 receivers randomly on a sphere shell that covers the inversion region D. Both the electric sources and the receivers are located in the middle layer, i.e., in the same layer as the object. This kind of measurement configuration is typical in ocean detection or atmosphere exploration. To simplify the calculation, we discrete the inversion region into $N_x \times N_y \times N_z = 11 \times 11 \times 11$ uniform cubic cells.

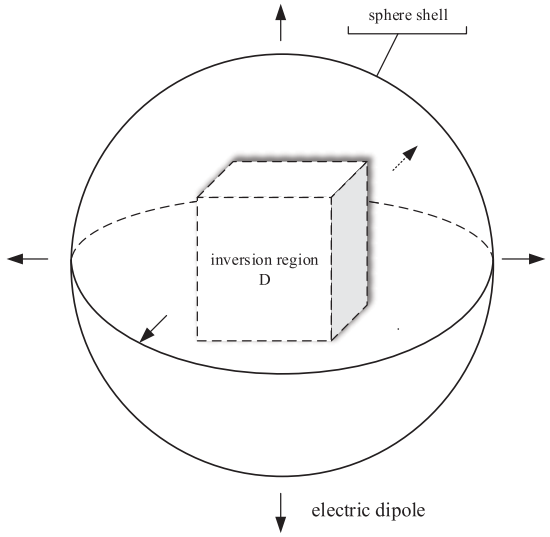

Fig. 2. Typical measurement configuration. Six electric dipoles are transmitters and illuminate the inversion region in six directions. The receivers randomly distribute in a sphere shell wrapping the inversion region.

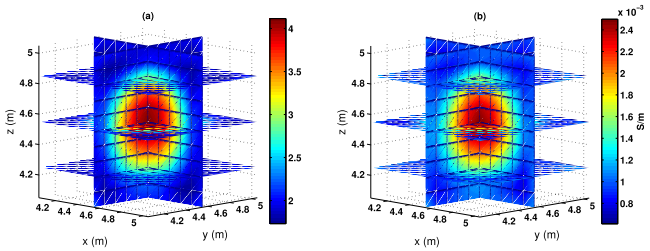

Fig. 3. Reconstructed results of a cubic object buried in spherically layered media. (a) Reconstructed relative permittivity. (b) Reconstructed conductivity.

The reconstructed results with the shading interpolations applied are illustrated in Fig. 3. We find that a very convincing identification of the location and the shape of the scatter can be obtained. The values of both permittivity and conductivity are around the true values. The REM is 11.6% for VBIM but increases to 14.3% when BIM is used. We also place the scatterer in the outermost layer and follow the same procedure to reconstruct it. The results are similar and not shown here.

B. Two Cubes Buried in the Middle Layer of a Three-Layered Medium

In order to validate the capability of our method in reconstructing multiple objects, we use the same parameters of the

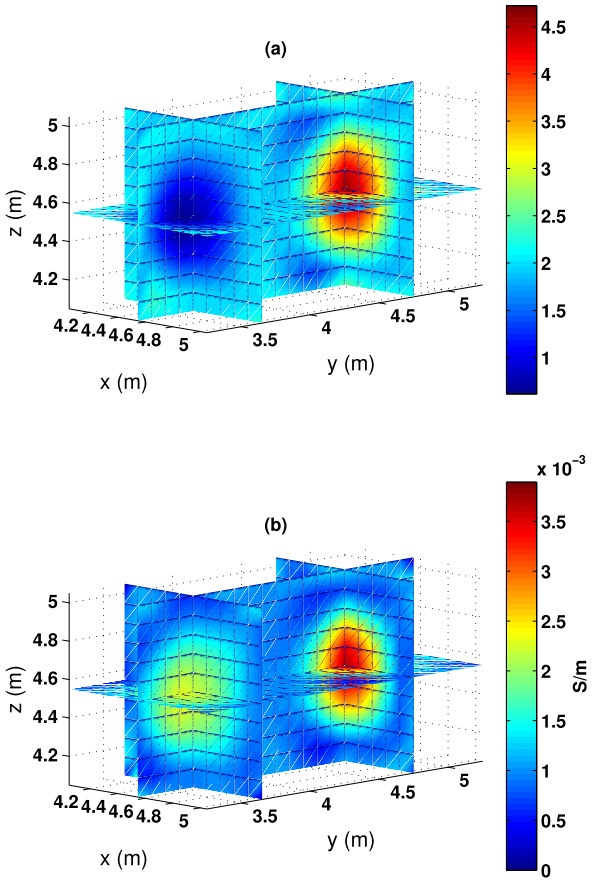

Fig. 4. Reconstructed results of two cubic scatterers buried in spherically layered media. (a) Reconstructed relative permittivity. (b) Reconstructed conductivity.

layered medium as in the last example, and place two cubic scatterers in the middle layer. The electrical parameters of one object are $\epsilon_{rx1} = 1.0$, $\mu_{rx1} = 1.0$, and $\sigma_{x1} = 0.002$ S/m, while those of the other one are $\epsilon_{rx2} = 4.0$, $\mu_{rx3} = 1.0$, and $\sigma_{x1} = 0.003$ S/m. The dimensions of the scatterers are $L_x = L_y = L_z = 0.5$ m. Their center coordinates are $(4.55, 3.6, 4.55)$ m and $(4.55, 4.7, 4.55)$ m, respectively. The inversion region D containing the scatterer has one lower corner located in $(4.0, 3.0, 4.0)$ m and the opposite upper corner located in $(5.1, 5.1, 5.1)$ m. In this case, we discretize the inversion region into $N_x \times N_y \times N_z = 11 \times 21 \times 11$ uniform cubic cells. The configuration of the transmitters and the receivers is similar to that in the last example. However, we increase the receiver number to 40 since the inversion region is larger than that in the last example, and thus the number of the unknowns in the discretized equation increases. The reconstructed permittivity and conductivity in the inversion region with the shading interpolations applied are shown in Fig. 4(a) and (b), respectively. The retrieved permittivity of the first cube is smaller than the background permittivity and that of the second one is larger than the background permittivity, as in the true model. We can see that both the permittivity and conductivity of the inversion region are close to the true values and reconstructed results show the exact locations of both scatterers. The REM for VBIM is 12.4%. However, the iteration is not convergent when BIM is used.

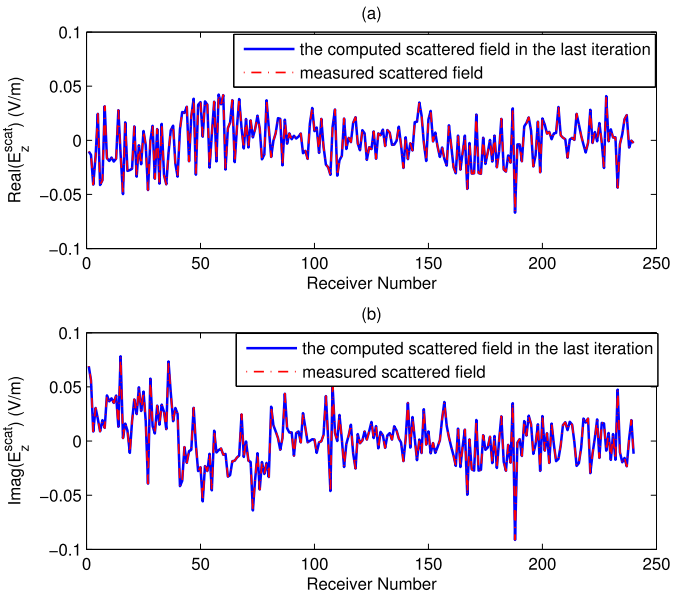

Fig. 5. Computed scattered field in the last iteration compared with measured scattered field. (a) Real parts of E_z^{scat} in receivers. (b) Imaginary parts of E_z^{scat} in receivers.

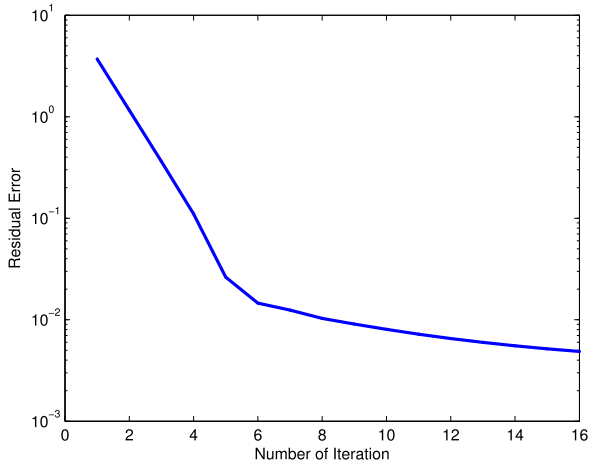

Fig. 6. Residual error of $\mathbf{E}^{\text{scat}}$ versus the number of iteration steps.

Fig. 5 shows the comparisons between the calculated scattered field in the last iteration and the measured scattered field excited by one electric dipole. Both the real and imaginary parts of scattered field E_z^{scat} show good agreements between the calculated and measured scattered fields. Other two components of scattered electric fields have similar agreements and are not shown here.

The relative residual error (RRE) of $\mathbf{E}^{\text{scat}}$ is defined as

$$\text{RRE} = \frac{\left|\left|\mathbf{E}_{\text{cal}}^{\text{scat}} - \mathbf{E}_{\text{meas}}^{\text{scat}}\right|\right|_{\text{Recs}}}{\left|\left|\mathbf{E}_{\text{meas}}^{\text{scat}}\right|\right|_{\text{Recs}}} \tag{13}$$

where $\mathbf{E}_{\text{meas}}^{\text{scat}}$ denotes the measured scattered fields in receivers and $\mathbf{E}_{\text{cal}}^{\text{scat}}$ stands for the computed scattered fields in each iteration in the receivers. Fig. 6 depicts the residual error between the calculated and measured scattered fields in the receivers versus the number of iterations steps. It only takes 16 iterations of our method to make the RRE less than 0.5%.

The VBIM works efficiently. It converges rapidly in the first several iterations and gradually become stable in the following steps.

Both examples are run on a computer with the CPU speed of 3.60 GHz and one core used. For the first example, it takes about 1 h 7 min to finish the forward solution, including the computation of Green's functions. For the inverse code with Green's functions precalculated, the elapsed time for each iteration is less than 1 min. In less than 10 min, the relative error of the scattered field drops lower than 0.5%. For the second example, the forward solver costs a little more than 10 h, while the inversion procedure consumes about 1 h and 20 min when the relative error of the scattered field drops lower than 0.5%. Note here we do not count the computation time of dyadic Green's functions when evaluating the inverse procedure. It is time consuming but only needs to be calculated once in VBIM.

Finally, we want to emphasize that we can also improve the accuracy of the retrieved parameters by increasing the receiver number. However, a larger number of receivers will lead to a huge cost in real application. And the numerical experiments show that the REM only decreases about 1% if we increase the receiver number to 500 in the second example.

IV. Conclusion

In this letter, we reconstruct the permittivity and conductivity of objects buried in spherically layered media using the VBIM. The forward solver employed here is provided by MOM combined with a Krylov subspace iterative method. Numerical experiments are used to validate the ability of VBIM in obtaining the location and size of multiple objects with a high resolution. The contribution of this letter is to provide an effective way to solve the inverse scattering problems in spherically layered media. However, in this letter, the computation cost is relatively high because the convolution between dyadic Green's functions and equivalent sources cannot be directly accelerated by Fast Fourier Transform (FFT) in spherically layered media. We only retrieved scatterers with the size smaller than $\lambda/10$. The high-resolution reconstruction of electrically large scatterers will cost huge computation time. In addition, stronger scattering from electrically larger objects will make the iteration more difficult to converge. The research focus in the future is the the rotational invariance of dyadic Green's functions and FFT applications in the spherically layered background media as well as their applications for the reconstruction of electrically large objects.

References

[1] T. J. Cui and W. C. Chew, "Novel diffraction tomographic algorithm for imaging two-dimensional dielectric objects buried under a lossy Earth," *IEEE Trans. Geosci. Remote Sens.*, vol. 38, no. 4, pp. 2033–2041, Jul. 2000.

[2] L. Poli, G. Oliveri, and A. Massa, "Microwave imaging within the first-order Born approximation by means of the contrast-field Bayesian compressive sensing," *IEEE Trans. Antennas Propag.*, vol. 60, no. 6, pp. 2865–2879, Jun. 2012.

[3] M. Ambrosanio and V. Pascazio, "A compressive-sensing-based approach for the detection and characterization of buried objects," *IEEE J. Sel. Topics Appl. Earth Observ. Remote Sens.*, vol. 8, no. 7, pp. 3386–3395, Jul. 2015.

[4] M. Bevacqua, L. Crocco, L. Di Donato, T. Isernia, and R. Palmeri, "Exploiting sparsity and field conditioning in subsurface microwave imaging of nonweak buried targets," *Radio Sci.*, vol. 51, no. 4, pp. 301–310, 2016.

[5] L. Crocco, I. Catapano, L. D. Donato, and T. Isernia, "The linear sampling method as a way to quantitative inverse scattering," *IEEE Trans. Antennas Propag.*, vol. 60, no. 4, pp. 1844–1853, Apr. 2012.

[6] A. Abubakar and P. M. van den Berg, "Three-dimensional inverse scattering applied to cross-well induction sensors," *IEEE Trans. Geosci. Remote Sens.*, vol. 38, no. 4, pp. 1669–1681, Jul. 2000.

[7] P. Rocca, G. Oliveri, and A. Massa, "Differential evolution as applied to electromagnetics," *IEEE Antennas Propag. Mag.*, vol. 53, no. 1, pp. 38–49, Feb. 2011.

[8] X. Chen, "Subspace-based optimization method for solving inverse-scattering problems," *IEEE Trans. Geosci. Remote Sens.*, vol. 48, no. 1, pp. 42–49, Jan. 2010.

[9] M. Pastorino and A. Randazzo, "Buried object detection by an inexact Newton method applied to nonlinear inverse scattering," *Int. J. Micro. Sci. Technol.*, vol. 2012, Jun. 2012.

[10] L. D. Donato, M. T. Bevacqua, L. Crocco, and T. Isernia, "Inverse scattering via virtual experiments and contrast source regularization," *IEEE Trans. Antennas Propag.*, vol. 63, no. 4, pp. 1669–1677, Apr. 2015.

[11] M. Li, O. Semerci, and A. Abubakar, "A contrast source inversion method in the wavelet domain," *Inv. Prob.*, vol. 29, no. 2, p. 025015, 2013.

[12] Y. M. Wang and W. C. Chew, "An iterative solution of the two-dimensional electromagnetic inverse scattering problem," *Int. J. Imag. Syst. Technol.*, vol. 1, no. 1, pp. 100–108, Jun. 1989.

[13] W. C. Chew and Y. M. Wang, "Reconstruction of two-dimensional permittivity distribution using the distorted Born iterative method," *IEEE Trans. Med. Imag.*, vol. 9, no. 2, pp. 218–225, Jun. 1990.

[14] C. Yu, M. Yuan, and Q. Liu, "Reconstruction of 3D objects from multifrequency experimental data with a fast DBIM-BCGS method," *Inverse Problems*, vol. 25, no. 2, p. 024007, Feb. 2009.

[15] N. Zaiping and Z. Yerong, "Hybrid Born iterative method in low-frequency inverse scattering problem," *IEEE Trans. Geosci. Remote Sens.*, vol. 36, no. 3, pp. 749–753, May 1998.

[16] N. Zaiping, Y. Feng, Z. Yanwen, and Z. Yerong, "Variational Born iteration method and its applications to hybrid inversion," *IEEE Trans. Geosci. Remote Sens.*, vol. 38, no. 4, pp. 1709–1715, Jul. 2000.

[17] W. Zhang and Q. H. Liu, "Three-dimensional scattering and inverse scattering from objects with simultaneous permittivity and permeability contrasts," *IEEE Trans. Geosci. Remote Sens.*, vol. 53, no. 1, pp. 429–439, Jan. 2015.

[18] F. Li, Q. H. Liu, and L.-P. Song, "Three-dimensional reconstruction of objects buried in layered media using Born and distorted Born iterative methods," *IEEE Geosci. Remote Sens. Lett.*, vol. 1, no. 2, pp. 107–111, Apr. 2004.

[19] L.-P. Song and Q. H. Liu, "Fast three-dimensional electromagnetic nonlinear inversion in layered media with a novel scattering approximation," *Inverse Problems*, vol. 20, no. 6, pp. S171–194, Dec. 2004.

[20] M. R. Hestenes and E. Stiefel, "Method of conjugate gradients for solving linear system," *J. Res. Nat. Bureau Standards*, vol. 49, no. 6, pp. 409–435, 1952.

[21] K. A. Michalski and D. Zheng, "Electromagnetic scattering and radiation by surfaces of arbitrary shape in layered media. II. Implementation and results for contiguous half-spaces," *IEEE Trans. Antennas Propag.*, vol. 38, no. 3, pp. 335–344, Mar. 1990.

[22] K. A. Michalski and D. Zheng, "Electromagnetic scattering and radiation by surface of arbitrary shape in layered media—Part II: Implementation and results for contiguous half-space," *IEEE Trans. Antennas Propagat.*, vol. 38, pp. 345–352, Mar. 1990.

[23] L.-W. Li, P.-S. Kooi, M.-S. Leong, and T.-S. Yee, "Electromagnetic dyadic Green's function in spherically multilayered media," *IEEE Trans. Microw. Theory Techn.*, vol. 42, no. 12, pp. 2302–2310, Dec. 1994.

[24] Y. Chen, F. Han, N. Liu, P. Wen, and Q. Liu, "Electromagnetic scattering from inhomogeneous objects embedded in spherically multilayered media solved by the method of moments," *Microw. Opt. Technol. Lett.*, vol. 59, no. 3, pp. 526–530, Mar. 2017.